Modification of Ag₃PO₄ surface using a nanosilver solution prepared under sunflower seed extract

Vania Amelia Azmi[a], Uyi Sulaeman[a,*], Rini Larasati[b], Dadan Hermawan[a], Ari Asnani[a], Isnaeni Isnaeni[c], Shu Yin[b,d]

[a]Department of Chemistry, Jenderal Soedirman University, Purwokerto 53122, Indonesia
[b]Institute of Multidisciplinary Research for Advanced Materials, Tohoku University, Sendai 9808577, Japan
[c]Research Center for Photonics, National Research, and Innovation Agency, Tangerang 15314, Indonesia
[d]Advanced Institute for Materials Research (WPI-AIMR), Tohoku University, Sendai 9808577, Japan

Abstract

Designing new properties of Ag₃PO₄ photocatalysts is challenging as the Ag₃PO₄ surface is highly susceptible to photocorrosion. This study aims to improve the properties of Ag₃PO₄ by modifying its surface using a nanosilver solution prepared under sunflower seed extract. This photocatalyst was prepared by chemical coprecipitation. Based on XPS analysis, the interaction of nanosilver solution with the Ag₃PO₄ surface significantly affected the P 2p chemical state and decreased the Ag/P atomic ratio of Ag₃PO₄. The modification of the Ag₃PO₄ surface by nanosilver solution resulted in the formation of silver vacancy defects and the incorporation of Ag nanoparticles (AgNPs) on the Ag₃PO₄ surface. This new design of Ag₃PO₄ showed a remarkable photocatalytic reaction for Rhodamine B oxidation and antibacterial activity under blue light irradiation. The photocatalytic reaction was mainly driven by forming superoxide anion radicals and hole species. This phenomenon can provide a new direction in the improvement of the photocatalytic ability of Ag₃PO₄ through a natural plant material approach.

Keywords: Ag₃PO₄; defect; nanosilver; silver vacancy; sunflower seed

1. Introduction

Recently, the modification of Ag₃PO₄ photocatalyst has been soaring rapidly. This phenomenon occurs in view of the unique properties of Ag₃PO₄ photocatalyst, which are capable of quickly degrading pollutants under visible radiation. The surface properties of this photocatalyst, however, are vulnerable and easily damaged by photoreduction. The root of the problem is that photoexcited electrons are able to reduce Ag^+ ions in Ag₃PO₄ to form Ag^0, leading to a decrease in the amount of Ag₃PO₄ photocatalyst, and making it no longer to have properties as a photocatalyst. This phenomenon is crucial for practical applications where the material is exposed to light for extended periods; many researchers, in turn, focus on addressing this drawback through heterostructure design such as band-band transfer [1,2], p-n heterojunction [3–5], and z-scheme mechanism [6–8]. These heterostructures are able to facilitate electron transfer and capture to prevent photo corrosion and charge recombination.

One of the promising approaches to prevent photoreduction and increase photocatalytic activity is the generation of Ag nanoparticles (AgNPs) in Ag₃PO₄ to form Ag/Ag₃PO₄ [9–11]. Silver nanoparticles can act as electron sinks [12], thereby preventing the recombination of electron-hole pairs generated during photocatalytic reactions. This then results in the increased availability of active species for chemical reactions. Incorporating nanosilver can modify the electronic structure of Ag₃PO₄, narrowing the band gap or forming new energy levels within the band gap. Also, it might result in the generation of surface plasmon resonance (SPR) [13], which can enhance light absorption and facilitate the separation of photogenerated electrons and holes. This design is an important breakthrough in synergistic effects in Ag₃PO₄-based composite materials [14,15].

The enhancement of the photocatalytic properties of silver phosphate can also be achieved by forming defects. The types of defects such as silver vacancy [16], phosphate deficiency [17], and substitutional ion [18] might be generated on the Ag₃PO₄ surface and can bring an impact on conductivity, reactivity, and overall stability of photocatalysts. Understanding and controlling them is deemed essential for optimizing the use of Ag₃PO₄ in various applications. Based on these principles, the defects generation on the Ag₃PO₄ surface

should be effectively designed to enhance its photocatalytic activities.

The incorporation of nanosilver and the presence of silver vacancy defects in Ag_3PO_4 have emerged as a significant area of concern for researchers [19,20]. This becomes a great opportunity to change the properties of photocatalysts because it combines the defects as charge traps and plasmon to enhance charge separation. This finding encourages further development to obtain an excellent Ag_3PO_4 photocatalyst with a different approach. In the current experiment, the incorporation of nanosilver and the formation of defects on Ag_3PO_4 have been successfully prepared using sunflower seed extract. The nanosilver solution was easily prepared through a reduction reaction of $AgNO_3$ using sunflower seed extract. This solution is useful not only for the formation of nanosilver metal dopants but also for inducing silver vacancies in Ag/Ag_3PO_4, which results in a highly active photocatalyst.

2. Materials and Methods

The analytical-grade chemicals used in this study were obtained from Merck including silver nitrate, disodium hydrogen phosphate dodecahydrate, benzoquinone, ammonium oxalate, isopropanol, sodium hydroxide, ferric chloride, rhodamine B (RhB), Nutrient Agar (NA), and Nutrient Broth (NB). The seeds of *Helianthus annuus*, commonly known as sunflower, were obtained from a local field.

2.1. Preparation of Sunflower seed extract

The sunflower seeds were washed with deionized water and dried in an oven for 24 hours. The dried seeds were then pulverized finely using a mortar and pestle. Subsequently, the sunflower seed aqueous extract was prepared by extracting 20 grams of fine seed powder in 100 milliliters of deionized water at room temperature for 24 hours. The extract solution was filtered and prepared for the incorporation of nanosilver.

2.2. Synthesis of defective Ag/Ag_3PO_4

The preparation of defective Ag/Ag_3PO_4 was conducted in three steps: preparation of nanosilver solution using sunflower extract, preparation of Ag_3PO_4 through the coprecipitation method of $AgNO_3$ and $Na_2HPO_4 \cdot 12H_2O$, and incorporation of AgNPs into Ag_3PO_4 crystals. The nanosilver solution was prepared by reacting 10 mL of 1 mM $AgNO_3$ solution with 1 mL of sunflower seed extract for 60 minutes (the higher absorption of nanosilver solution). The solution was then centrifuged at 9000 rpm for 10 minutes to remove any remaining impurities. In the second step, the Ag_3PO_4 material was prepared by mixing an $AgNO_3$ solution (1.69 grams in 10 mL of deionized water) and a $Na_2HPO_4 \cdot 12H_2O$ solution (2 grams in 20 mL of deionized water) to form a yellow precipitate, which was then washed with deionized water. The reaction was conducted by the dropwise addition of phosphate solution to the silver ion solution. In the third step, the synthesized Ag_3PO_4 material was suspended with nanosilver solution sonicated for 5 minutes and aged for 24 hours in a dark room. The formed precipitate was washed with deionized water and dried at 60°C for 5 hours. Ag_3PO_4 prepared with nanosilver solution was named as the AP-Ag sample, while the sample that did not undergo nanosilver solution treatment was labelled as the AP sample. The nanosilver was also separated for characterization and was labelled as "Ag".

2.3. Characterization

The samples of Ag, AP, and AP-Ag were characterized by means of Bruker D2 Phaser X-ray diffraction equipment with a 1.5418 Å Cu Kα radiation source. Rietveld refinement was applied in High Score Plus software for the XRD data analysis. A variety of optical analyses were used to characterize the AP and AP-Ag sample: UV-Vis DRS (Jasco, V-600), FTIR (Thermo Scientific Nicolet iS10), Raman spectroscopy (Jasco, RMP-500DSEII), and PL spectra (Ocean Optics, MAYAPRO2000). Meanwhile, the morphology was investigated using FE-SEM (Hitachi, S-4800) and the chemical state of the surface was analyzed using XPS (ULVAC-PHI, PHI5600).

2.4. Photocatalytic activity evaluation

The photocatalytic activity was evaluated through Rhodamine B oxidation under blue light exposure (LED lamp 3 W, Ranpo) [17]. The RhB solution (100 mL, 10 mg/L) was added with 100 mg of photocatalyst and sonicated to facilitate the distribution of the photocatalyst. The reaction was conducted by magnetic stirring in the dark for 20 minutes to ensure equilibrium between adsorption and desorption and a photocatalytic reaction was carried out. RhB solution samples (3 mL) were collected every 3 minutes followed by centrifugation (10000 rpm, 10 min) to separate the supernatant. A spectrophotometer here was utilized to analyze the concentration of RhB. To examine the reactive species, 1 mL of a 0.025 M scavenger was introduced to the photocatalytic processes, wherein $\cdot O_2^-$, h^+, and $\cdot OH$ were respectively trapped by benzoquinone (BQ), ammonium oxalate (AO), and isopropanol (IPA) [21]. The material's photostability was evaluated through four cycles of the photocatalytic reaction.

2.5. Antibacterial activity

Antibacterial activity was evaluated against two different bacteria, *S. aureus* (gram-positive bacteria) and *E. coli* (gram-negative bacteria) under dark and irradiation conditions. The antibacterial properties of the material were investigated using the well diffusion method [22]. Petri dishes here were prepared with 15 mL of NA and wells were created using a 4 mm and 6 mm crock drill bit to accommodate the material. A bacterial colony (1 mL) was streaked on the plate. Subsequently, 30 μL of the material was added to the well, and the bacteria were incubated at 37°C for 24 hours. The antibacterial activity was examined under two distinct conditions; those are in a dark room and under blue light irradiation.

3. Results and Discussion

3.1. Characterization of the materials

The formation of AgNPs was achieved through the

reduction of AgNO₃ in the presence of sunflower extract. The formation of AgNPs was monitored using a UV-visible spectrophotometer. The formation of AgNPs has been recognized to be capable of producing the surface plasmon resonance (SPR) in a visible region [23]. Figure 1(a) illustrates the reactions conducted at 20, 40, and 60 min to obtain AgNPs. A broad absorption of 350-550 nm was observed after treatment with sunflower extract. This phenomenon indicated that the SPR of AgNPs was successfully generated. The higher absorption was obtained after 60 min of reaction suggesting that the reaction time is an important role in the synthesis of AgNPs.
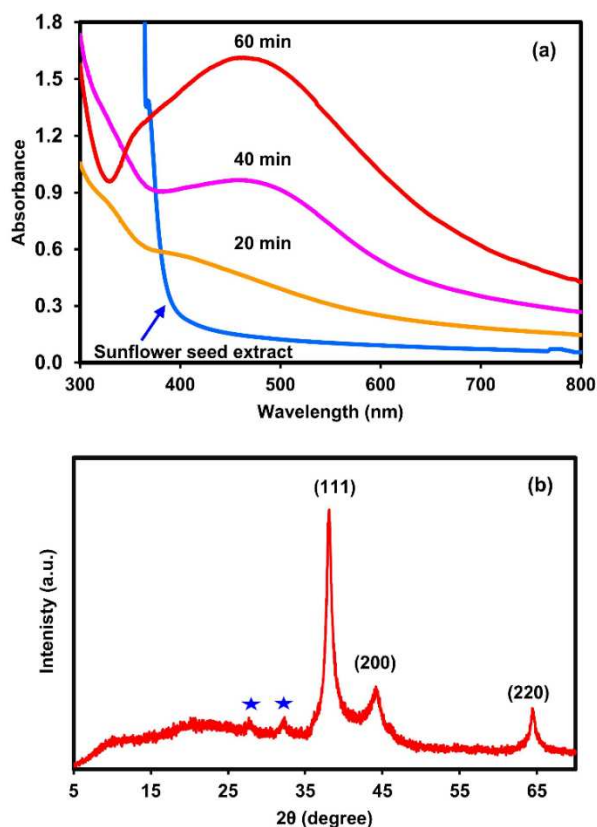

Fig. 1. The UV-Vis absorption of Ag⁺ reduction using sunflower extract with varying reaction time (a), and XRD of Ag nanoparticles (AgNPs) (b)

The product of AgNPs was analyzed using XRD and High score plus with Rietveld refinement. Bragg diffraction peaks (2θ) of 38.0893°, 44.2541°, and 64.3268° were indexed to (111), (200), and (220) planes (Fig. 1(b)). These peaks matched the cubic structure (COD: 96-110-0137) with the space group of Fm-3m (225). The XRD results clearly showed that the AgNPs were crystalline. The XRD data unequivocally demonstrated the crystalline of the AgNPs. Furthermore, the diameter of AgNPs was estimated using the Debye-Scherer principle [24]. The crystallite diameter of AgNPs was estimated to be around 6.49 nm. Two peaks of impurities (marked with a star) were observed, indicating that the AgNPs surface was where the bio-organic phase crystallizes. These findings are comparable to those reported for silver nanoparticles prepared using *Coleus aromaticus* leaf extract [24].

Fig. 2(a) depicts the Ag₃PO₄ with nanosilver solution treatment generated under sunflower extract (AP-Ag) and Ag₃PO₄ (AP) as control. All observed peak diffractions were

matched with the reference data (COD number 90-101-0606) with the space group of P-43n (218). A minor peak of AgNPs (111) was observed in AP-Ag, indicating that a small quantity of Ag might be incorporated on the Ag₃PO₄ surface (Fig. 2(b)). The shift of 2θ was observed after treatment with a nanosilver solution. To make it clearer, the 2θ of the 110-plane decreased from 20.8635° (AP) to 20.8348° (AP-Ag) (Fig. 2(c)) indicating that the d-space of 110-plane in the AP sample (4.2543 Å) increased to 4.2601 Å in the sample of AP-Ag. The increase of d-space might be induced by nanosilver and organic compounds in sunflower aqueous extract. Considering the small amount of nanosilver incorporated on the Ag₃PO₄ surface, the significant increase in d-space was most likely due to defect formation rather than nanosilver dopant. These defects were probably more due to organic compounds from sunflower seed extract.
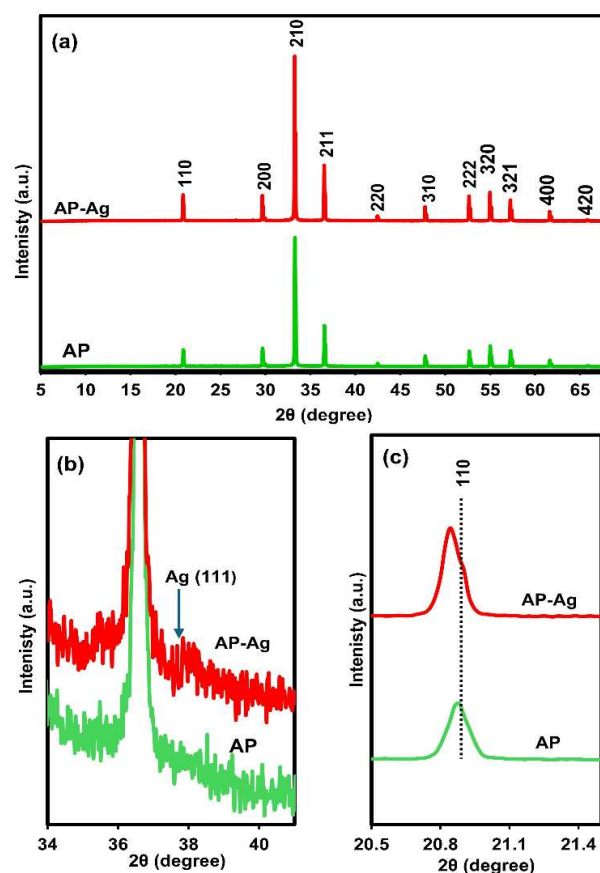

Fig. 2. The XRD of Ag₃PO₄ (AP) and Ag₃PO₄ treated with nanosilver solution (AP-Ag) (a), the identification of 111-plane for nanosilver (b), and the shift of 110-plane diffraction of Ag₃PO₄ (c)

The morphology of AP and AP-Ag was investigated through SEM analysis (Fig. 3 (a,b)). An irregular sphere morphology of samples was observed in both AP and AP-Ag. The particle sizes from 0.5 to 2.0 μm were found in both AP and AP-Ag samples. Besides irregular, a rhombic dodecahedral was observed in AP-Ag, indicating that the aging treatment under nanosilver significantly changed the morphology of the Ag₃PO₄ surface. The elemental analysis of AP-Ag was also carried out to evaluate the distribution of elements in photocatalyst (Fig. 3(c,d,e)). The elemental analysis revealed a uniform distribution of silver, phosphorus, and oxygen elements in the AP-Ag samples.
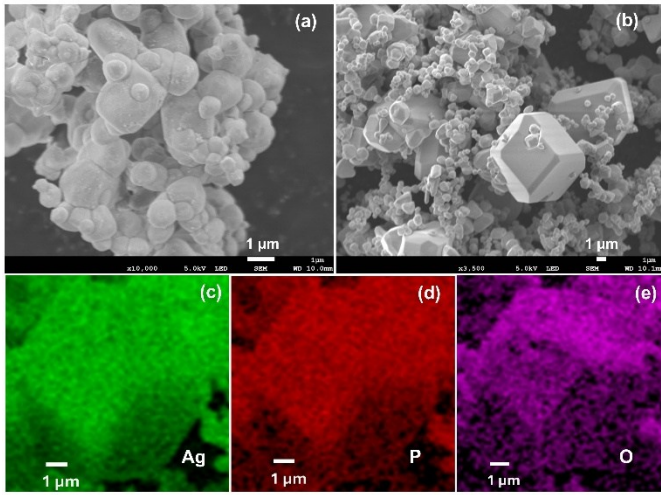
Fig. 3. SEM images of AP (a), AP-Ag (b) with the elemental analysis of silver (c), phosphor (d), and oxygen (e)
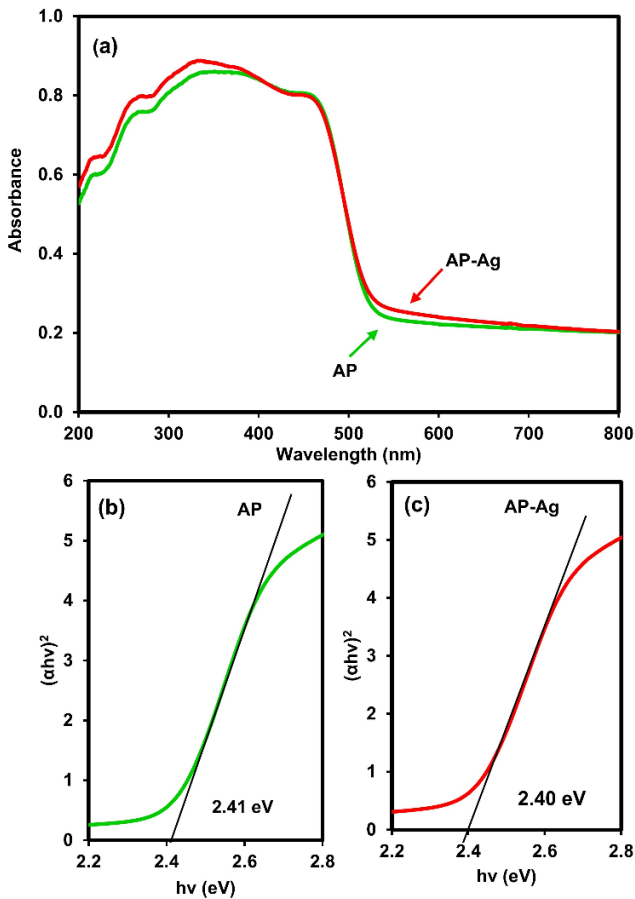

Fig. 4. UV-Vis DRS absorption (a), band gap energy determination using Tauc plot for AP (b) and AP-Ag (c)

The optical absorption characteristics of materials were measured by UV-Vis DRS and the results are presented in Fig. 4(a). A slightly increased absorption of 500-700 nm was observed in AP-Ag. The band gap (Eg) of each material was determined using Eq. (1) (Tauc plot).

$$\alpha h\upsilon = A(h\upsilon - Eg)^{n/2} \tag{1}$$

The symbols α, h, and υ refer to the absorption coefficient,

Planck's constant, and the light frequency, respectively [16]. The value of n varies depending on whether it is an indirect (n = 4) or direct (n = 1) transition, and A is a value of constant. Based on this equation, the direct band gap energies of AP and AP-Ag were found at 2.41 eV and 2.40 eV, respectively (Fig. 4(b,c)). The slight increase in absorption and reduction in bandgap energy of AP-Ag suggests that the nanosilver solution in sunflower seed extract affected the optical properties. These phenomena might be caused by the defect generation of Ag_3PO_4 on the surface due to the interaction of nanosilver and organic molecules in sunflower extract with the phosphate group of the Ag_3PO_4.
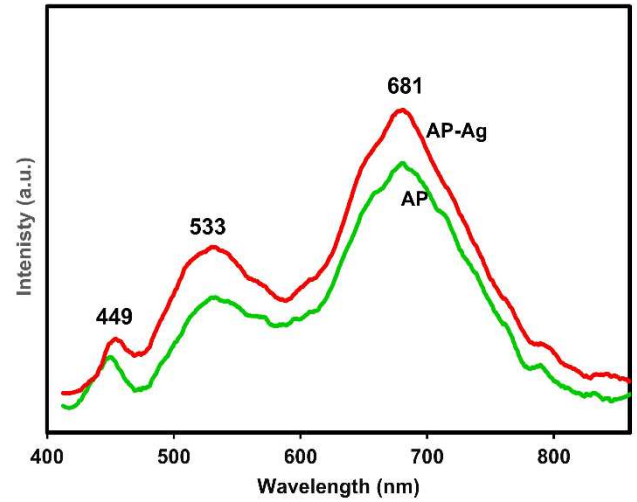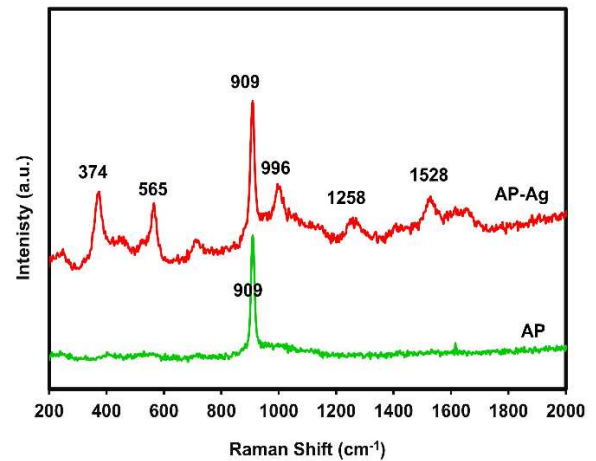

Fig. 5. PL spectra of AP and AP-Ag samples

Fig. 6. Raman spectra of AP and AP-Ag

The photogenerated electron and hole recombination were evaluated by PL spectra analysis (Fig. 5). The emission of 449 nm, 533 nm, and 681 nm was recorded after the excitation at 405 nm using an LED laser. These emissions were associated with the energy transition of 2.76, 2.33, and 1.82 eV, respectively. These transitions might correspond with new band edge transition, band gap of Ag_3PO_4, and natural defect sites, respectively. Of these emissions, the natural defect site of 1.82 eV was found as the highest emission, which was responsible for the high recombination of photogenerated charges. Upon treatment with nanosilver solution, the PL

intensity increased, indicating that the modified Ag_3PO_4 may have more photo-excited electrons, and when these electrons returned to the ground state, the PL spectrum increased.

The new properties of AP-Ag were recognized by Raman spectrophotometer analysis (Fig. 6). A sharp band of 909 cm^{-1} was observed in AP, which was assigned to $[PO_4]$ symmetric stretching vibrations [25]. The sample of AP-Ag exhibited many bands of 374, 565, 909, 996, 1258, and 1528 cm^{-1}, showing the new properties of the AP-Ag. This is a special property of Ag_3PO_4 in which the Raman peak at 565 cm^{-1} is ascribed to P-O-P bonds symmetric stretching [26], and the peak of 996 cm^{-1} originates from the anti-symmetric stretching of $[PO_4]$ tetrahedra [27]. The peaks of 1258 and 1528 cm^{-1} are linked to the CH_2 twisting [28] and C=C stretching vibration [29], which are the characteristics of organic compounds from sunflower seed extract. These incorporations could change the properties of Ag_3PO_4.
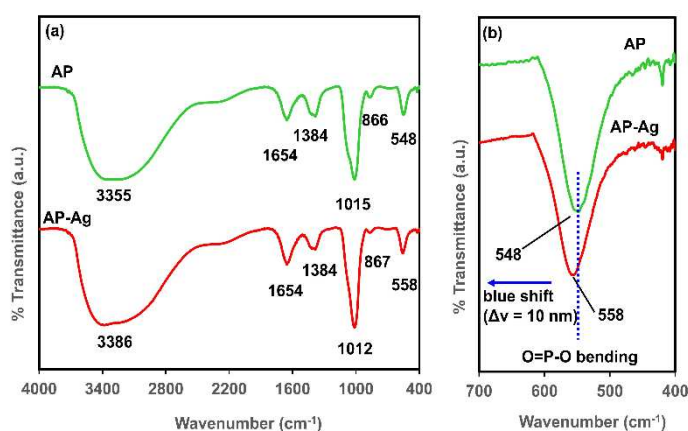

Fig. 7. (a) The FTIR of AP and AP-Ag (a), and blue shift of O=P-O bending (b)

Fig. 7(a) displays the FTIR spectra of the AP and AP-Ag samples. The AP sample demonstrated that the broad peaks at 3355 and 1654 cm^{-1}, respectively, were linked to the stretching and bending of O–H and H–O–H vibrations, thereby confirming the presence of adsorbed water molecules on the sample. The stretching of the P=O vibration was observed at the band at 1384 cm^{-1}. The antisymmetric of PO_4 stretching was linked to the strongest absorption peak at 1015 cm^{-1}. The bending vibrations of the O=P–O bond were responsible for the band at 548 cm^{-1}, whereas the symmetric stretching vibrations of the P–O–P bond were linked to the band at 866 cm^{-1}. These observed FTIR spectra are in accordance with the findings of other studies [27]. The bending of the O=P–O vibrations in AP-Ag shifted to higher energy (blue shift) (Fig. 7(b)), suggesting that the nanosilver treatment altered the phosphate functional group feature on the Ag_3PO_4 surface.

The interaction of nanosilver solution created under sunflower seed extract was investigated using XPS. The binding energies (BEs) of 373.90 eV and 367.88 eV, which were assigned to Ag^+ $3d_{3/2}$ and Ag^+ $3d_{5/2}$, respectively [30], were observed in the AP sample (Fig. 8(a)). These peaks decreased to 373.79 eV and 367.77 eV after treatment with nanosilver solution (AP-Ag). The small peak of metallic nanosilver (Ag^0) could be observed from the deconvolution of the AP-Ag sample, showing the BEs of 375.11 eV and 368.88

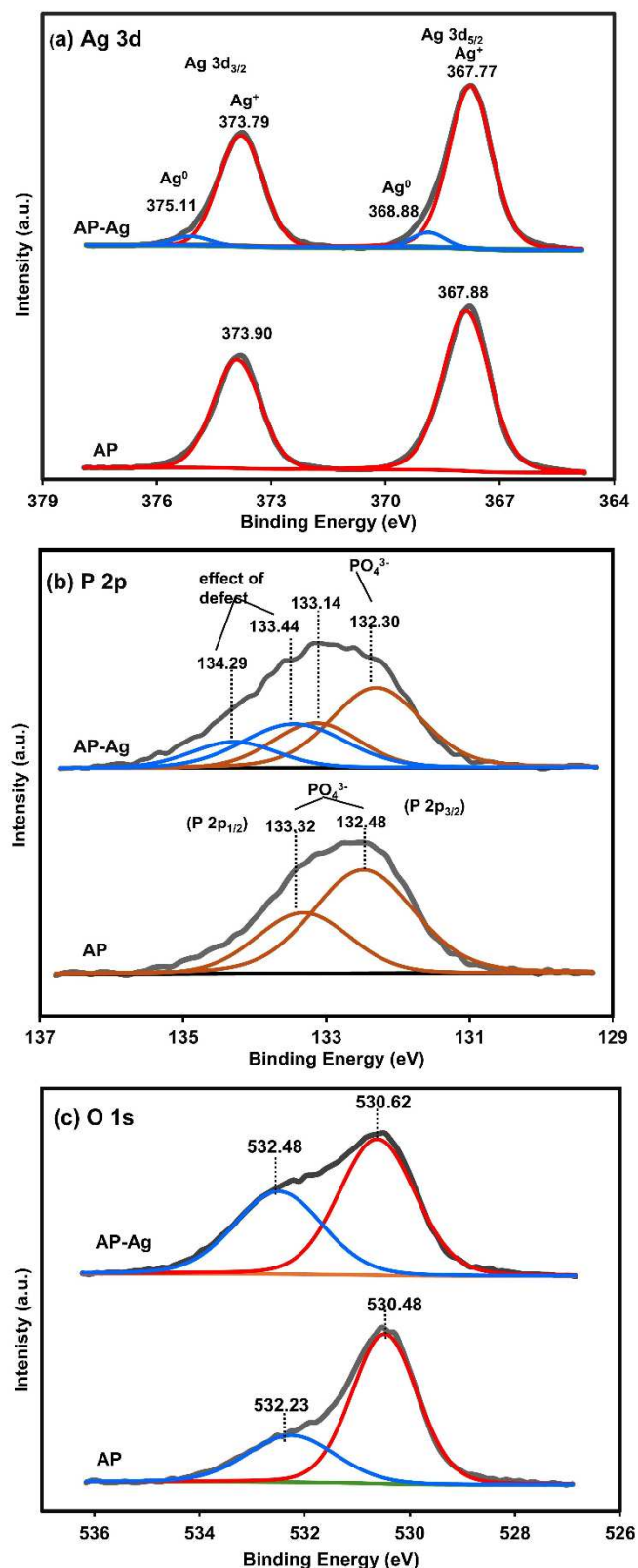eV for $Ag3d_{3/2}$ and $Ag3d_{5/2}$ respectively [31].

Fig. 8. XPS deconvolution of Ag 3d (a), P 2p (b), and O 1s (c) for AP and AP-Ag

The most significant alterations were observed in the P 2p spectrum. The BEs of 133.32 eV and 132.48 eV associated with P $2p_{1/2}$ and P $2p_{3/2}$, respectively [30] were found in the AP sample. After treatment with nanosilver solution (AP-Ag), the

broadening of the P 2p spectrum was significantly observed. The deconvolution analysis revealed that P 2p of AP-Ag had two chemical states as illustrated in Fig. 8(b). The new chemical states of 134.29 eV and 133.44 eV, which were assigned to P $2p_{1/2}$ and P $2p_{3/2}$, respectively, may have originated from defect formation. Both the nanosilver and the compounds in the sunflower seed extract solution may react with the phosphate group on the Ag_3PO_4 surface, forming the defect sites.

The spectra of O 1s in the AP sample can be deconvoluted into two spectra of 532.23 eV and 530.48 eV (Fig. 8(c)). The peak at 530.48 eV was associated with the oxygen of Ag_3PO_4 and other peak at 532.23 eV originated from the –OH or H_2O adsorbed on the Ag_3PO_4 surface [32]. The BEs of O1s in AP-Ag were slightly increased. The peak intensity of 532.48 eV was higher in AP-Ag, suggesting that the oxygen from the organic compound might also be adsorbed on the surface of Ag_3PO_4.
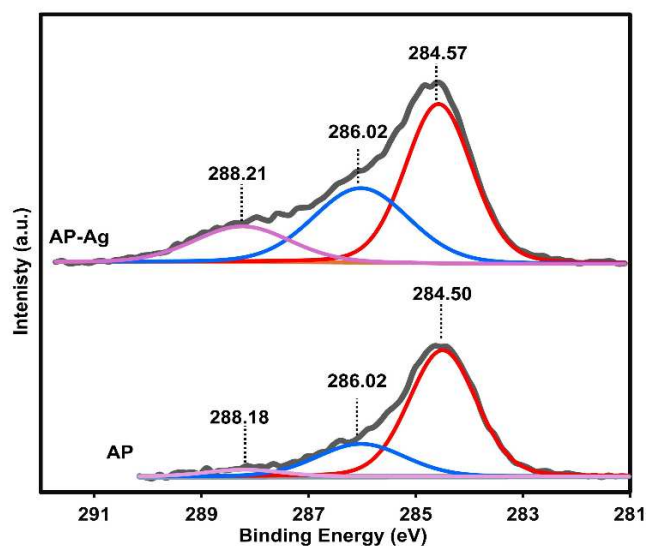

Fig. 9. XPS deconvolution of C 1s for AP and AP-Ag

The deconvolution of C 1s in the AP sample yielded three peaks, centered at 284.50, 286.02, and 288.18 eV, which were attributed to C–C/C–H, C–O, and O–C=O, respectively (Fig. 9) [33]. In an atmospheric environment, carbon is easily adsorbed in the Ag_3PO_4 sample. The intensity of C1s in AP-Ag increased significantly, indicating that organic molecules in the extract were also chemically adsorbed on the Ag_3PO_4 surface. The peaks centered at 284.57, 286.02, and 288.21 eV in the AP-Ag sample were attributed to C–C/C–H, C–O, and O–C=O, respectively [33]. The peak intensity of C 1s in AP-Ag increased, indicating that a greater quantity of organic carbon was adsorbed on the Ag_3PO_4 surface.

Table 1. Atomic ratios of the samples analyzed using XPS

Samples	Atomic ratios			
	Ag/P	Ag/O	O_T/P	O_L/P
AP	2.75	0.739	3.72	2.60
AP-Ag	1.94	0.437	4.43	2.60

O_T is the oxygen total in the sample
O_L is the oxygen lattice of Ag_3PO_4

Defect analysis can be investigated using atomic ratio calculation (Table 1). The Ag/P atomic ratios of 2.75 and 1.94 were obtained in AP and AP-Ag samples, respectively. The significant decrease of Ag/P in AP-Ag implied that nanosilver solution treatment caused silver vacancy in the sample. Silver vacancy in AP-Ag was also supported by the decrease of the Ag/O atomic ratio. Silver vacancies were easily formed in Ag_3PO_4 crystals compared to oxygen vacancies. The strong covalent bond between P and O could prevent the formation of oxygen vacancies in Ag_3PO_4 crystals. After nanosilver treatment, the O_L/P ratio remained unaltered (2.60), indicating that the P-O bond was quite strong.

3.2. The photocatalytic activities

The photocatalytic activities of Ag, AP, and AP-Ag were tested through the oxidation of RhB under blue light exposure. The photocatalytic abilities are shown in Fig. 10(a).
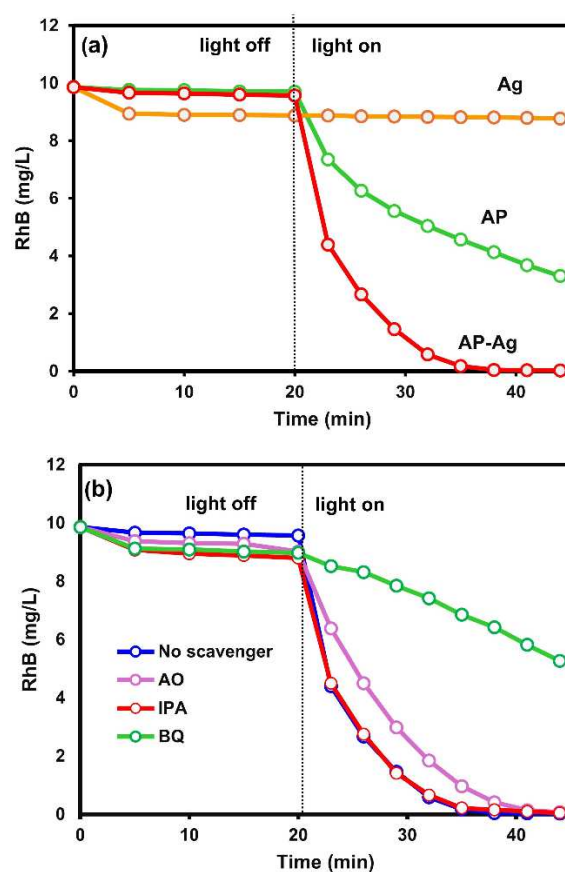

Fig. 10. The photocatalytic activity of samples for Rhodamine B oxidation (a) and the active species investigation in the AP-Ag sample (b)

After 20 minutes in the dark and 15 minutes of irradiation, the AP-Ag sample exhibited the highest RhB removal ability, reaching 98.20%. In comparison, the Ag and AP samples demonstrated significantly lower removal abilities with the values of 10.56% and 53.66%, respectively. A pseudo-first-order kinetics model was also used to study photocatalytic reaction's kinetics. This model was represented by the equation $\ln(C_0/C_t) = kt$, where C_0, C_t, k, and t are the initial RhB concentration, the RhB concentration at a given irradiation time, the rate constant, and the irradiation time, respectively [33]. Based on this equation, the rate constants of 0.0005,

0.0558, and 0.2430 min^{-1} were found in Ag, AP, and AP-Ag, respectively. The photocatalytic activity of AP-Ag increased 4.35 times compared to the AP sample.

The active species on the Ag$_3$PO$_4$ surface were also investigated using a scavenger. The scavenger benzoquinone (BQ), ammonium oxalate (AO), and isopropanol (IPA) were utilized to capture the superoxide ion radicals (•O$_2^-$), holes (h$^+$), and hydroxyl radicals (•OH) respectively [21]. The analysis of active species is presented in Fig. 10(b). The addition of IPA to the reaction did not decrease photocatalytic activity, indicating no active hydroxyl radical species on the surface of the photocatalyst. In contrast, the addition of AO and BQ significantly decreased the photocatalytic activity, indicating that the photocatalytic reaction was driven by the formation of active hole species and superoxide radical ions, respectively. The superoxide ion radicals exhibited the highest role in the photocatalytic reaction.
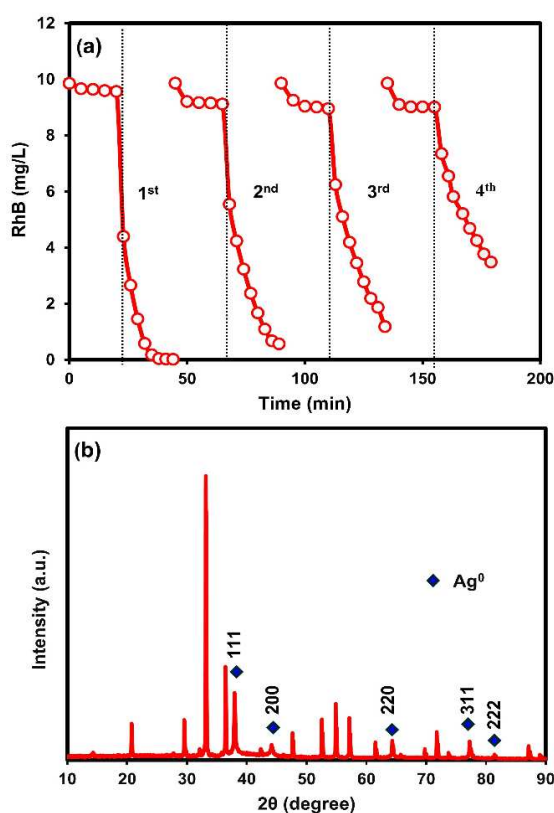
The photocatalytic reaction decreased gradually after the cyclic test, indicating the possibility of photoreduction. To understand this phenomenon, the sample subjected to four cyclic tests was analyzed using XRD that revealed the formation of the metallic silver (Ag^0) (Fig. 11(b)). It implied that the Ag$^+$ ion in Ag$_3$PO$_4$ has been reduced to Ag^0 during light irradiation leading to a photocorrosion in Ag$_3$PO$_4$, resulting in lower photocatalytic activities [17].

3.3. Antibacterial activity

Fig. 12 (a,b) presents the diameter of zones of inhibition (ZOI) of the Ag, AP, and AP-Ag samples against those bacteria pathogen. Under dark conditions, the ZOI was observed at 2.3 mm, 6.62 mm, and 8.38 mm against S. aureus for Ag, AP, and AP-Ag samples, respectively. Their ZOI diameter then increased to 2.84 mm, 8.84 mm, and 9.87 mm under irradiation for Ag, AP, and AP-Ag respectively. The sample of AP-Ag exhibited higher antibacterial activity against *S. aureus* in both dark and irradiation conditions.

Fig. 11. Cyclic reaction evaluation (a), and XRD profile after four-cycle reaction (b)
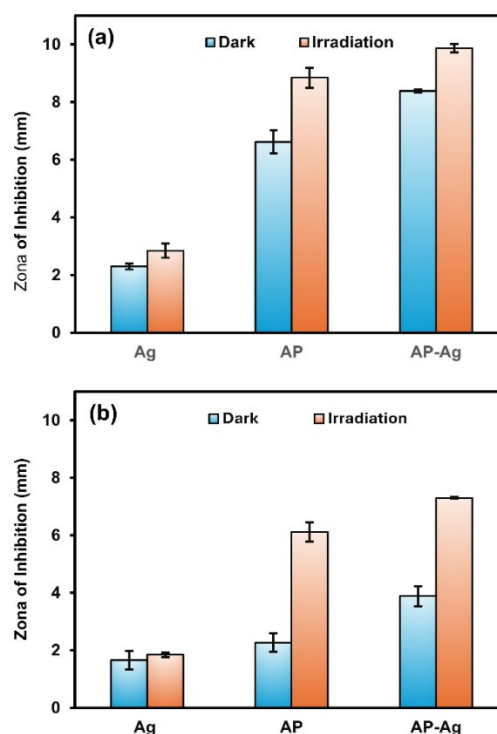
Fig. 12. Measurement of zones of inhibition against (a) *S. aureus*, (b) *E. coli*

As depicted in Fig. 13, the photocatalytic mechanism can be explained as follows. The photocatalyst material contains silver vacancies and AgNPs dopants. Upon irradiation with blue light, electrons in the valence band (VB) are excited to the conduction band (CB) resulting in the formation of holes in the VB and photo-excited electrons in the CB. The photo-excited electrons can be transferred to AgNPs, accelerating the reduction of O$_2$ to •O$_2^-$. Meanwhile, the holes can oxidize the RhB compound to CO$_2$ and H$_2$O. The silver vacancies can facilitate the migration of holes, which can enhance the oxidation reaction.

The photostability of AP-Ag was also evaluated over four cycles of reaction and the results are presented in Fig. 11(a).

Fig. 13. Mechanism of photocatalytic activities in AP-Ag (Ag/Ag$_3$PO$_4$) for Rhodamine B degradation and bacterial inhibition

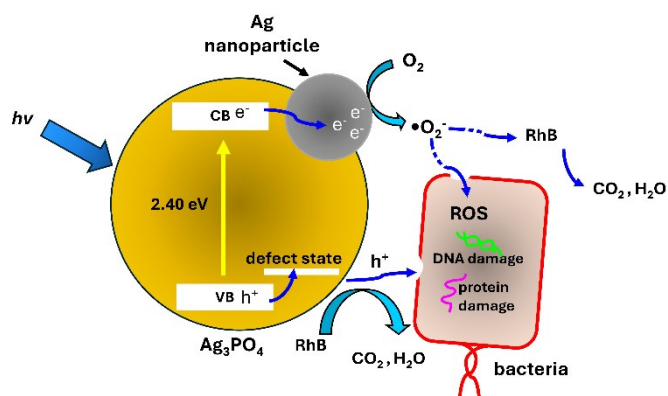The ZOI diameter observed against *E. coli* under dark conditions was 1.66 mm, 2.27 mm, and 3.88 mm for Ag, AP, and AP-Ag, respectively. The ZOI diameter increased to 1.84 mm, 6.12 mm, and 7.3 mm under irradiation. The results demonstrated that the light irradiation on AP and AP-Ag photocatalysts had a significant effect on *E. Coli*, indicating that ROS (reactive oxygen species) are more active in inhibiting *E. coli*. [34]. This is because *E. coli* is a gram-negative bacterium that has a thinner peptidoglycan layer on its cell walls with an outer membrane of lipopolysaccharides; therefore, it is more susceptible to photocatalytic active species. The increased ZOIs observed in AP-Ag may be related to higher surface defects. Surface defects induced reactive sites for Ag_3PO_4 to interact with microorganisms leading to an increase of antibacterial properties. A similar phenomenon of defect photocatalyst with high antibacterial activity was also found in ZnO [35].

The mechanism of bacteria inhibition in AP-Ag photocatalysis is illustrated in Fig. 13. Upon blue light irradiation, holes and electrons could be generated in VB and CB, respectively. Holes might be trapped in defect states while photoexcited electrons in CB were transferred to AgNPs, which could enhance the formation of superoxide radicals. This phenomenon produced reactive oxygen species (ROS), which caused cell membrane disruption and damage to DNA and proteins. In addition, holes play a role in oxidizing cell membranes, resulting in higher bacterial inactivation.

4. Conclusion

The synthesis of nanosilver was successfully achieved through the reduction of $AgNO_3$ in the presence of sunflower seed extract. The modification of the Ag_3PO_4 surface under sunflower seed extract resulted in defective Ag/Ag_3PO_4. It can be concluded that nanosilver and organic compound in the sunflower extract solution are capable of interacting with the Ag_3PO_4 surface, thereby altering the bending vibration of the O=P–O bond, the chemical state of P 2p, and atomic ratio of Ag/P. This phenomenon results in the release of Ag^+ ions from the surface, thereby creating a silver vacancy in Ag_3PO_4. The new properties of Ag_3PO_4 exhibited excellent photocatalytic ability under blue light irradiation and enhanced antibacterial activity against both *S. aureus* and *E. coli*. The enhanced reactivity at the modified Ag_3PO_4 surface was attributed to superoxide radicals and holes at the surface during irradiation.

Acknowledgments

References

1. W. Zhang, S.C. Li, M. Yan, L. Li, J. Ma, J. Wang et al., *In-situ oxidation selective deposition of tetrahedral Ag₃PO₄{111} on monoclinic BiVO₄{040} with highly efficient visible light-driven photocatalysis and long recycling*, J. Environ. Chem. Eng. 10 (2022) 108418.

2. H.H. Abed and S.H. Ammar, *Building of a ternary AgI/ZIF-8/g-C₃N₄ heterojunction for efficient photodecomposition of organic pollutants in batch and split-plate airlift reactors*, Case Stud. Chem. Environ. Eng. 10 (2024) 100909.

3. X. Zhang, C. Chen, T. Cheng, Y. Tian, M. Wen, B. Hou et al., *Construction highly efficient p–n heterojunctions composite of BiBaO₃ and Ag₃PO₄ for visible light driven photocatalytic degradation of tetracycline and oxytetracycline*, Water Resour. Ind. 31 (2024) 100246.

4. Y. Wu, Y. Luo, C. Yang and Q. Wu, *Enhanced efficiency of interfacial charge transfer in Ag₃PO₄/BiPO₄@CNTs photocatalyst for amoxicillin degradation: Synergistic effect of p-n heterojunction and conjugated channels*, Surf. Interfaces 51 (2024) 104801.

5. S. Pahi, B. Mahapatra, A. Behera, S.K. Singh and R.K. Patel, *Fermi level induced band edge alignment and band bending in Ag₃PO₄/Cu₂O p-n heterojunction for proficient photocatalytic applications*, Mater. Chem. Phys. 305 (2023) 127992.

6. O. Oyegbeda, S.O. Akpotu and B. Moodley, *A novel Z-scheme covalent triazine framework/silver phosphate (CTF/Ag₃PO₄) heterojunction photocatalyst: Improved adsorption, photocatalytic degradation and degradation mechanism of rifampicin*, J. Environ. Chem. Eng. 12 (2024) 113447.

7. Z. Fu, K. Ye, Z. Dong, S. Li, H. Zhou, S. Xia et al., *Lattice matched Z-scheme ZnIn₂S₄/Ag₃PO₄ enhanced photocatalytic performance by controlling morphology synthesis*, J. Environ. Chem. Eng. 12 (2024) 113427.

8. N. Ding, Q. Fei, D. Xiao, H. Zhang, H. Yin, C. Yuan et al., *Highly efficient and recyclable Z-scheme heterojunction of Ag₃PO₄/g-C₃N₄ floating foam for photocatalytic inactivation of harmful algae under visible light*, Chemosphere 317 (2023) 137773.

9. Y. Dai, Y. Wang, G. Zuo, J. Kong, Y. Guo, C. Sun et al., *Photodegradation of acenaphthylene over plasmonic Ag/Ag₃PO₄ nanopolyhedrons synthesized via in-situ reduction*, Appl. Surf. Sci. 572 (2022) 151421.

10. X. Ren, G. Hu, Q. Guo, D. Gao, L. Wang and X. Hu, *Ag/Ag₃PO₄ nanoparticles assembled on sepiolite nanofibers: Enhanced visible-light-driven photocatalysis and the important role of Ag decoration*, Mater. Sci. Semicond. Process 156 (2023) 107272.

11. S. Zhang, C. Lei and L. Song, *Chiral induction enhanced photocatalytic degradation of methyl orange by Ag@Ag₃PO₄ and the reaction mechanism,* Ceram. Int. 49 (2023) 26548–26557.

12. P.J. Mafa, R. Patala, B.B. Mamba, D. Liu, J. Gui, A.T. Kuvarega, Plasmonic Ag₃PO₄/EG photoanode for visible light-driven photoelectrocatalytic degradation of diuretic drug, Chem. Eng. J. 393 (2020) 124804.

13. T. Du, C. Hu, Y. Li, Y. Pang, M. Li, B. Liu et al., *High-efficiency photocatalytic degradation of Rhodamine B and tetracycline by Z-scheme nanostructured Ag/Ag₃PO₄/Ti³⁺-TiO₂ mesocrystals heterojunctions under visible light*, Mater. Sci. Semicond. Process 172 (2024) 108081.

14. C. Zhang, X. Ni, W. Xu, J. Chen, L. Wang, R. Liu et al., *Highly efficient visible-light photocatalyst Ag/Ag₃PO₄/Bi₂O₂CO₃ enabled by the synergistic effect of heterojunction and surface plasma resonance*, Mater. Sci. Semicond. Process 166 (2023) 107704.

15. F. Liu, Y. Wang, S. Zhang, F. Sun, D. Xu, W. Wang et al., *Enhanced ultraviolet–visible–near infrared driven photocatalytic activity of 1D/0D BiVO₄:Er/Yb@Ag/Ag₃PO₄ Z-scheme heterostructure via a synergetic strategy of plasmonic effect and upconversion luminescence*, Ceram. Int. 49 (2023) 26589–26603.

16. U. Sulaeman, D. Hermawan, R. Andreas, A.Z. Abdullah and S. Yin, *Native defects in silver orthophosphate and their effects on photocatalytic activity under visible light irradiation*, Appl. Surf. Sci. 428 (2018) 1029–1035.

17. U. Sulaeman, R. Larasati, D.A.R.W. Putri, D. Hermawan, A. Asnani, I.

Isnaeni et al., *Design of defective silver phosphate photocatalyst using Nigella sativa seed aqueous extract for enhanced photocatalytic activity*, Inorg. Chem. Commun. 163 (2024) 112368.

18. Y. Huang, T. Ma, Q.Y. Chen, C. Cao and Y. He, *The electronic properties of impurities (N, C, F, Cl, and S) in Ag₃PO₄: A hybrid functional method study*, Sci. Rep. 5 (2015) 12750.

19. R. Liu, H. Li, L. Duan, H. Shen, Q. Zhang and X. Zhao, *The synergistic effect of graphene oxide and silver vacancy in Ag₃PO₄-based photocatalysts for rhodamine B degradation under visible light*, Appl. Surf. Sci. 462 (2018) 263–269.

20. X. Liu, J. Xu, T. Zhang, J. Zhang, D. Xia, Y. Du et al. *Construction of Ag nanocluster-modified Ag₃PO₄ containing silver vacancies via in-situ reduction: With enhancing the photocatalytic degradation activity of sulfamethoxazole*, J. Colloid. Interface Sci. 629 (2023) 989–1002.

21. V.G. Deonikar, R.B. Mujmule, D.R. Patil and H. Kim, *Efficient decontamination of toxic phenol pollutant using LaCO₃OH nanowires decorated Ag₃PO₄ hierarchical composites mediated by metallic Ag*, Sci. Total Environ. 675 (2019) 325–336.

22. G. Chavez-Esquivel, H. Cervantes-Cuevas, L.F. Ybieta-Olvera, M.T. Castañeda Briones, D. Acosta and J. Cabello, *Antimicrobial activity of graphite oxide doped with silver against Bacillus subtilis, Candida albicans, Escherichia coli, and Staphylococcus aureus by agar well diffusion test: Synthesis and characterization*, Mater. Sci. Eng. C 123 (2021) 111934.

23. K. Sharma, S. Guleria and V.K. Razdan, *Green synthesis of silver nanoparticles using Ocimum gratissimum leaf extract: characterization, antimicrobial activity and toxicity analysis*, J. Plant Biochem. Biotechnol. 29 (2020) 213–224.

24. M. Vanaja and G. Annadurai, *Coleus aromaticus leaf extract mediated synthesis of silver nanoparticles and its bactericidal activity*, Appl. Nanosci. 3 (2013) 217–223.

25. K. Dânoun, R. Tabit, A. Laghzizil and M. Zahouily, *A novel approach for the synthesis of nanostructured Ag₃PO₄ from phosphate rock: high catalytic and antibacterial activities*, BMC Chem. 15 (2021) 42.

26. L. Liu, Y. Qi, J. Lu, S. Lin, W. An, Y. Liang et al., *A stable Ag₃PO₄@g-C₃N₄ hybrid core@shell composite with enhanced visible light photocatalytic degradation*, Appl. Catal. B 183 (2016) 133–141.

27. J.V.B. Moura, C.D. de Abreu Lima, E.A.O. Melo, V.E. Santos, W.C. Ferreira, P.T.C. Freire et al., *Temperature-dependent phonon dynamics of Ag₃PO₄ microcrystals,* Spectrochim. Acta A Mol. Biomol. Spectrosc. 249 (2021) 119339.

28. P. Partovi-Azar and T.D. Kühne, *Full assignment of ab-initio Raman spectra at finite temperatures using Wannier polarizabilities: Application to cyclohexane molecule in gas phase*, Micromachines 12 (2021) 1212.

29. D.B. Powell, J.G.V. Scott and N. Sheppard, *Infrared and Raman spectra and the νC=C stretching frequencies of some silver-olefin and platinum-olefin complexes*, Spectrochim. Acta A: Mol. Spectrosc. 28 (1972) 327–335.

30. Z. Liu, Y. Liu, P. Xu, Z. Ma, J. Wang and H. Yuan, *Rational design of wide spectral-responsive heterostructures of Au nanorod coupled Ag₃PO₄ with enhanced photocatalytic performance,* ACS Appl. Mater. Interfaces 9 (2017) 20620–20629.

31. U. Sulaeman, S. Suhendar, H. Diastuti, R. Andreas and S. Yin, *Design of defect and metallic silver in silver phosphate photocatalyst using the hydroxyapatite and glucose*, Indones. J. Chem. 20 (2020) 1441–1447.

32. S.A. Chang, P.Y. Wen, T. Wu and Y.W. Lin, *Microwave-assisted synthesis of chalcopyrite/silver phosphate composites with enhanced degradation of rhodamine b under photo-fenton process*, Nanomater. 10 (2020) 2300.

33. O. Pop-Georgievski, D. Kubies, J. Zemek, N. Neykova, R. Demianchuk, E.M. Chánová et al., *Self-assembled anchor layers/polysaccharide coatings on titanium surfaces: A study of functionalization and stability*, Beilstein J. Nanotechnol. 6 (2015) 617–631.

34. S. Ninganagouda, V. Rathod, D. Singh, J. Hiremath, A.K. Singh, J. Mathew et al., *Growth kinetics and mechanistic action of reactive oxygen species released by silver nanoparticles from Aspergillus niger on Escherichia coli*, Biomed Res. Int. 2014 (2014) 753419.

35. I.S. Okeke, K.K. Agwu, A.A. Ubachukwu, I.G. Madiba, M. Maaza, G.M. Whyte et al., *Impact of particle size and surface defects on antibacterial and photocatalytic activities of undoped and Mg-doped ZnO nanoparticles, biosynthesized using one-step simple process*, Vacuum 187 (2021) 110110.